Applied Catalysis B: Environmental 181 (2016) 838–847

Contents lists available at ScienceDirect

Applied Catalysis B: Environmental

journal homepage: www.elsevier.com/locate/apcatb

A facile synthesis of CdSe quantum dots-decorated anatase TiO_2 with exposed {0 0 1} facets and its superior photocatalytic activity

Peng Wang, Xiao Li, Jialin Fang, Danzhen Li*, Jing Chen, Xiaoyun Zhang, Yu Shao, Yunhui He

Research Institute of Photocatalysis, State Key Laboratory of Photocatalysis on Energy and Environment, Fuzhou University, Fuzhou 350002, PR China

ARTICLE INFO

Article history:
Received 18 June 2015
Received in revised form 25 August 2015
Accepted 29 August 2015
Available online 1 September 2015

Keywords:
CS-T001
Photocatalytic reduction
Highly efficient
Nitro aromatics
Visible light

ABSTRACT

Anatase TiO_2 with exposed {0 0 1} facets (denoted as T001) is becoming one of the hotspots in photocatalytic field due to the highly reactive {0 0 1} facets. Nowadays, to further extend the applications of T001 in visible region, researchers are struggling to develop T001-based visible-light-responsive photocatalysts. In this paper, for the first time, CdSe quantum dots (QDs)-decorated T001 (denoted as CS-T001) was synthesized successfully via a facile method and demonstrated as a highly efficient and stable photocatalyst for reduction of nitro aromatics under visible light irradiation. Besides the obviously extended light absorption in visible region, the decoration of CdSe QDs onto T001 would remarkably improve the transfer and separation efficiency of photogenerated charge carriers, resulting in the much higher activity of CS-T001 as compared with pure T001 and CdSe QDs. Serving as the accepted sites for photoelectrons generated from CdSe QDs, the substrate T001 also plays a vital role. First, T001 offers highly active reaction sites due to the much higher surface energy of {0 0 1} facet than that of {1 0 1} facet. Second, compared with CdSe QDs-decorated anatase TiO_2 with exposed {1 0 1} facets (denoted as CS-T101), CS-T001 can generate electrons with stronger reducibility to participate in the photocatalytic reduction process. Third, the aggregation of T001 nanosheets gives rise to the porous structures with slit-like pores, providing efficient transport pathways to reactant and product molecules. Fourth, CS-T001 possesses much higher separation efficiency of photogenerated charge carriers as compared to CS-T101. We believe that our work could not only provide a facile method for fabricating novel QDs-decorated T001 photocatalysts but also help us to realize the synergy between decoration of QDs and exposure of TiO_2 {0 0 1} facets during the photocatalytic reaction process.

1. Introduction

In 2008, Yang and his colleagues successfully synthesized micro-sized anatase TiO_2 crystals with approximately 47% of highly reactive {0 0 1} facets [1]. It has stimulated worldwide research interest in the preparation of anatase TiO_2 with exposed {0 0 1} facets (denoted as T001) and its application in photocatalytic field. Both theoretical and experimental studies demonstrate that the {0 0 1} facet of anatase TiO_2 is much more reactive than the thermodynamically more stable {1 0 1} facet [2–4]. Due to the high ratio of the exposed {0 0 1} facets, T001 has been reported to exhibit superior activity in many aspects of photocatalytic field [5–10]. Although enhanced photocatalytic activity can be obtained by increasing the percentage of {0 0 1} facets, T001 can be excited only under ultravoilet (UV) light irradiation owing to the large band gap of TiO_2. In order to make full use of visible light which accounts for the major part of solar light, it is essential to develop novel T001-based photocatalysts which can work efficiently under a wide range of visible light irradiation.

Generally, the photoresponse of T001 can be extended to visible region through the following strategies. Metal or non-metal ions doping of T001 can tune its electronic structure and thus obtain visible-light-responsive photocatalysts [11–14]. However, the dopants can easily become the recombination centers for charge carriers and lower stability of the doped materials. Deposition of transition or noble metals onto T001 is an effectively strategy to enhance visible light photocatalytic activity [15–20]. Nevertheless, metal clusters at a higher concentration will also serve as a recombination center for electron–hole pairs, which noticeably decreases the photocatalytic activity.

By contrast, sensitization by narrow band gap semiconductor is a more feasible route to enhance the visible light photocatalytic

* Corresponding author. Fax: +86 591 83779256.
E-mail address: dzli@fzu.edu.cn (D. Li).

http://dx.doi.org/10.1016/j.apcatb.2015.08.046
0926-3373/

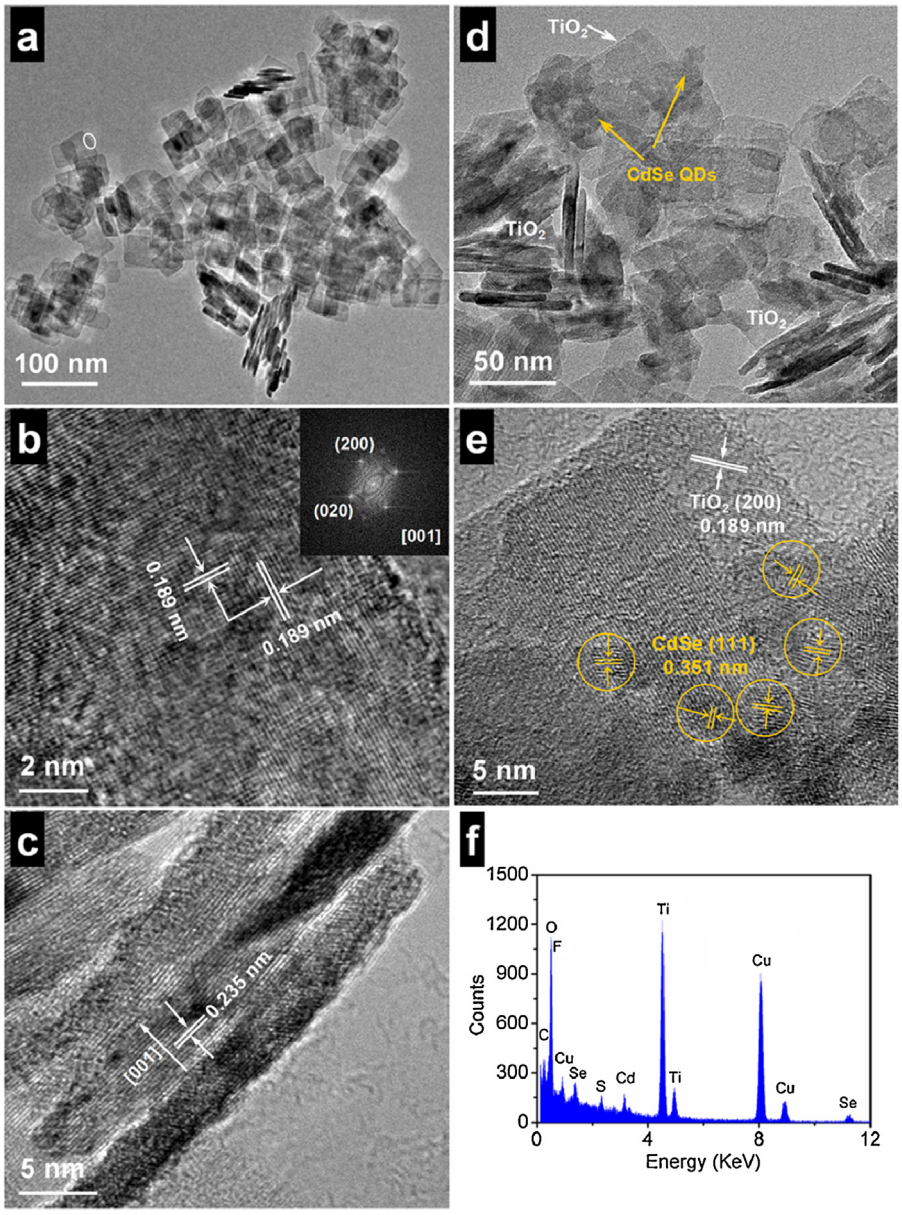

Fig. 1. The TEM (a), HRTEM (b and c) images and corresponding FFT image (inset) of T001; the TEM (d), HRTEM (e) images and EDX pattern (f) of 5%CS-T001.

activity of T001 [21–23]. Besides the obvious visible light response, the heterojunction formed by T001 and narrow band gap semiconductor contributes significantly to the efficient separation of charge carriers. Especially for semiconductor quantum dots (QDs) decorated T001, the fast diffusion of charge carriers across the interface will cause the rapid charge transfer between QDs and T001, leading to the greatly enhanced photocatalytic activity [24–26]. Due to the obvious quantum size effect, strong capability for visible light absorption and well matched energy band position with TiO_2, CdSe QDs has been extensively employed to couple with TiO_2 in the field of photoelectrochemical devices, solar cells and photocatalysis [27–34]. However, to the best of our knowledge, the work on coupling T001 with CdSe QDs in photocatalytic field has not been reported up to now.

As a kind of important intermediates of dyes, medicines and organic light-emitting diodes, amino aromatics are typically synthesized by reduction of nitro aromatics. Recently, owing to the mild reaction condition, environmentally friendliness and low cost, photocatalysis technique has become a new feasible and promising approach for the reduction of nitro aromatics [35–38]. As is known, TiO_2 has shown great potential as an ideal and powerful photocatalyst for various significant reactions. It has been reported that TiO_2 is also active for the photocatalytic reduction of nitro aromatics [37,39–41]. However, the possible re-oxidation of amino group of amino aromatics and the shortage of UV light-responsive for TiO_2 become the obstacles to its further application [41]. So it is well worth ameliorating the photocatalytic performance of TiO_2 for reduction of nitro aromatics, especially under visible light irradiation.

In this work, we successfully synthesized CdSe QDs-decorated T001 (denoted as CS-T001) photocatalyst via a facile method for the first time. The results demonstrated that the CS-T001 exhibited highly efficient photocatalytic activities for reduction of nitro aromatics under visible light irradiation. Among all samples, including T001, CdSe QDs, $TiO_{2-x}N_x$, CS-T001, CdSe QDs-decorated commercial TiO_2 (Degussa P25) (denoted as CS-P25) and CdSe QDs-decorated anatase TiO_2 with exposed {1 0 1} facets (denoted as CS-T101), the CS-T001 showed the best activity. The possible

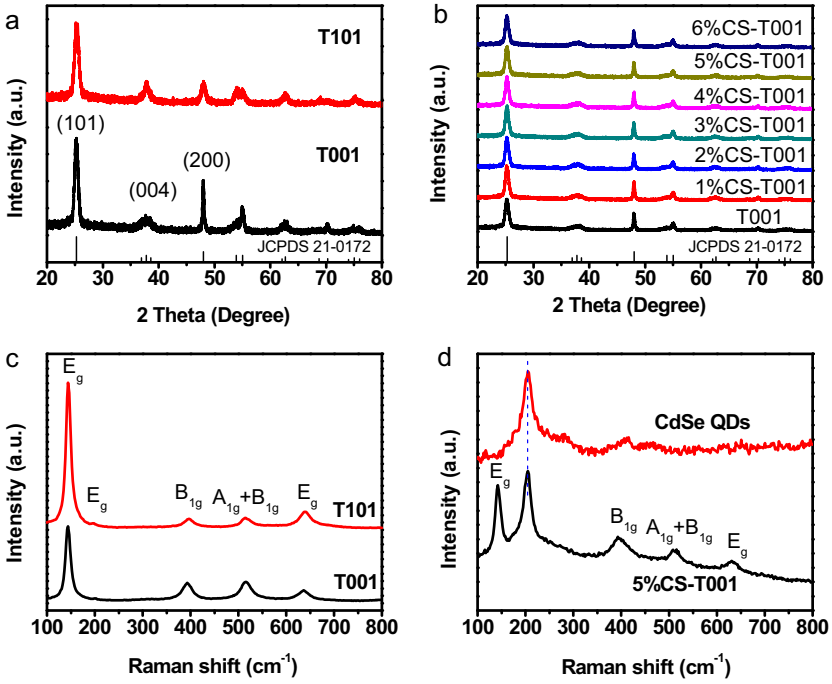

Fig. 2. XRD patterns of T001, T101 (a) and CS-T001 with different contents of CdSe QDs (b); Raman spectra of T001, T101 (c) and CdSe QDs, 5%CS-T001 (d).

reasons and involved factors for the enhancement of photocatalytic performance over CS-T001 were discussed in detail, and the reaction mechanism of photocatalytic reduction was proposed consequently.

2. Experimental

2.1. Materials

$CdCl_2{\cdot}2.5H_2O$ (99.99%), sodium borohydride ($NaBH_4$) were purchased from the Shanghai Chemical Co.. Selenium powder (Se, 99%), mercaptoacetic acid (MAA) was supplied by Aladdin-reagent. Sodium sulfite (Na_2SO_3) was from Yongjia Chemical Reagent Factory. Tetrabutyl titanate ($Ti(OBu)_4$, 98%), hydrofluoric acid (47%), ethanol, hydrochloric acid, sodium hydroxide, 4-nitroaniline (4-NA), 3-nitroaniline (3-NA), 2-nitroaniline (2-NA), 4-nitrotoluene and 4-nitrophenol were purchased from Sinopharm Chemical Reagent Co., Ltd., Commercial TiO_2 (P25) was kindly supplied by Degussa Company. All chemicals were analytical grade and used without further purification, and all experiments were carried out using deionized water.

2.2. Preparation of samples

2.2.1. Preparation of water soluble CdSe QDs

CdSe QDs were prepared by aqueous synthesis method according to our previous report [42]. Typically, 2 mmol of $CdCl_2{\cdot}2.5H_2O$ was dissolved in 200 mL of deionized water in a three-necked flask and was deaerated with N_2 bubbling for 1 h. Then 230 μL of stabilizer (MAA) was added to the solution above. The pH value of the solution was adjusted to 11 with 1 M NaOH aqueous solution. Oxygen-free NaHSe solution was prepared by mixing 0.1053 g of Se powder and 0.3160 g of $NaBH_4$ into 5 mL of deionized water under N_2 atmosphere. Then the freshly prepared oxygen-free NaHSe solution was quickly injected into the N_2 saturated Cd^{2+} solution under vigorous stirring. The initial molar ratio of Cd^{2+}: Se^{2-}: MAA was 3:2:5. After refluxing at 80 °C for 4 h, the desired orange–red colored water-soluble CdSe QDs solution was obtained. In addition, to precipitate CdSe QDs, equal volume of ethanol was added into the above solution under stirring. The precipitated CdSe QDs powder was separated by centrifugation, further washed with deionized water and ethanol for several times, and dried in vacuum at 60 °C.

2.2.2. Preparation of T001 and T101

T001 was prepared using a hydrothermal method similar to that described by Han et al. [5]. In a typical preparation procedure, 25 mL of $Ti(OC_4H_9)_4$ and 3 mL of hydrofluoric acid solution were mixed in a dried Teflon-lined autoclave with a capacity of 100 mL at room temperature, and then kept at 180 °C for 24 h. After hydrothermal reaction, the white precipitates were collected, washed with ethanol and deionized water for three times, and then dried in an oven at 80 °C for 6 h.

For comparison, anatase TiO_2 with exposed {1 0 1} facets (denoted as T101) was synthesized under the same conditions by using 3 mL of deionized water instead of hydrofluoric acid.

2.2.3. Preparation of CS-T001, CS-T101, CS-P25 and $TiO_{2-x}N_x$

The sample 5%CS-T001 was prepared through a facile hybridization method. T001-H_2O suspension was prepared by dispersing 0.5 g of T001 into 100 mL of H_2O. Then the pH value of 22 mL of CdSe QDs solution was adjusted to 6.0 with 1 M HCl aqueous solution. After that, the above CdSe QDs solution was mixed with T001-H_2O suspension and stirred for 24 h. The products were centrifuged and washed with deionized water and ethanol for several times, and finally dried in vacuum at 60 °C for several hours. CS-T001 with different contents of CdSe QDs from 1% to 6% were obtained by varying the volume of CdSe QDs solution.

For comparison, CS-T101 and CS-P25 were prepared under the same conditions by replacing T001 with T101 and P25, respectively. Additionally, N-doped TiO_2 was synthesized by traditional method [43], which was designated as $TiO_{2-x}N_x$.

2.3. Characterization

The crystal structures of samples were determined by using a Bruker D8 Advance X-ray diffractometer at 40 kV and 40 mA with

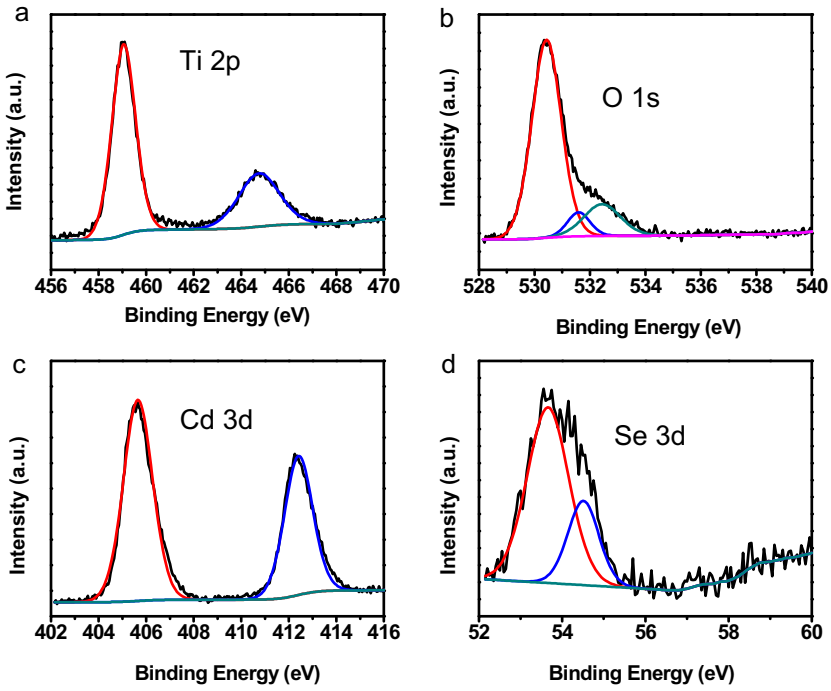

Fig. 3. High-resolution XPS spectra of the Ti 2p (a), O 1s (b), Cd 3d (c) and Se 3d (d) regions for 5%CS-T001.

Ni-filtered Cu Kα radiation in the 2θ ranging from 20° to 80° with a scan rate of 0.02°/s. The diffuse reflectance spectroscopy (DRS) of the samples were characterized by a Varian Cary 500 Scan UV-vis-NIR spectrometer with $BaSO_4$ as the background ranging from 200 to 800 nm. Edinburgh FL/FS900 fluorescence spectrometer was used to investigate the photoluminescence (PL) spectra for samples. The transmission electron microscope (TEM), high-resolution transmission electron microscope (HRTEM) and energy dispersive X-ray spectrum (EDX) were recorded on a FEI Tecnai G2 F20 instrument operated at an accelerating voltage of 200 kV. Raman spectroscopy was recorded at room temperature on a Renishaw invia Raman System and equipped with the 785 nm line of an Ar ion laser as an excitation source. X-ray photoelectron spectroscopy (XPS) spectra were acquired using an ESCALAB 250 photoelectron spectrometer (Thermo Fisher Scientific) at 3.0×10^{-10} m bar with monochromatic Al Kα radiation (E = 1486.2 eV). All of the binding energies were calibrated by the C 1s peak at 284.6 eV. The Brunauer–Emmett–Teller (BET) specific surface area and porosity of the samples were measured on a Micromeritics ASAP2020 analyzer by N_2 adsorption at 77 K. All photoelectrochemical tests were carried out in a conventional three-electrode cell filled with 0.1 M of Na_2SO_4 electrolyte (30 mL). A Pt plate was used as the counter electrode, and an Ag/AgCl/sat. KCl electrode was used as the reference electrode. The sample was deposited as a film formed on a 5 mm × 5 mm indium-tin-oxide (ITO) conductive glass that served as the working electrode. Mott-Schottky experiments were conducted on a Precision PARC workstation and the potential ranged from 0.1 V to 1.1 V vs. Ag/AgCl). The perturbation signal was 20 mV with a frequency of 1000 Hz. The photocurrent and electrochemical impedance spectroscopy (EIS) were both measured on a CHI-660D electrochemical workstation (Chenhua Instruments, Co., Shanghai). The transient photocurrent vs. time plots were measured at bias of 0 V vs. Ag/AgCl under visible light irradiation with on/off light cycles of 20 s intervals. The EIS measurement was carried out in the frequency ranging from 10^5 to 0.1 Hz with amplitude of 5 mV at a bias potential of 0 V vs. Ag/AgCl. Electron paramagnetic resonance (EPR) was used to detect radicals spin-trapped by 5,5-dimethyl-L-pyrroline N-oxide (DMPO). The signals were collected by a Bruker model A300 spectrometer (Bruker Instruments, Inc.) with the settings of center field (3512 G), microwave frequency (9.86 GHz), and power (20 mW).

2.4. Measurements of photocatalytic activity

The photocatalytic reduction of nitro aromatics was conducted in an aqueous solution under visible light irradiation. The light source was a 500 W Xe-arc lamp (CEL-S500 Beijing China Education Au-light Co., Ltd.) with a 420–800 nm band-pass filter. All the photocatalytic experiments were conducted at a light energy density of 0.20 W/cm^2. Prior to the photocatalytic test, 80 mg of photocatalyst was suspended in 80 mL of nitro aromatic aqueous solution (20 mg/L) in a 100-mL Pyrex glass vessel. After adding 20 mg of Na_2SO_3 as holes scavenger, the suspensions were magnetically stirred in dark for 1 h in order to reach adsorption–desorption equilibrium between the sample and nitro aromatics. At given time intervals, 3 mL of sample solution was collected and centrifuged to remove the catalyst. Then the supernatants were analyzed on a Varian Cary 50 UV–vis spectrophotometer. The whole photocatalytic process was carried out under N_2 bubbling at a flow rate of 80 mL/min. Conversion of the nitro aromatics is defined as follows: conversion (%) = $[(C_0 - C)/C_0] \times 100$, where C_0 is the initial concentration of nitro aromatics and C is the concentration of nitro aromatics at a certain time interval after photocatalytic reaction.

3. Results and discussion

3.1. Characterization of samples

The morphologies and microstructures of samples were characterized by TEM. Fig. 1a presents a typical TEM image of pure T001. It consists of sheet-shaped structures having a rectangular outline with an average side length of about 40–70 nm and thickness of about 4–6 nm. By comparison, Fig. S1 shows that T001 is composed of nanoparticles with crystal size of about 10–20 nm. Fig. 1b shows the high-resolution (HR)TEM image of a single nanosheet of T001 obtained from the white framed area in Fig. 1a. Two sets of

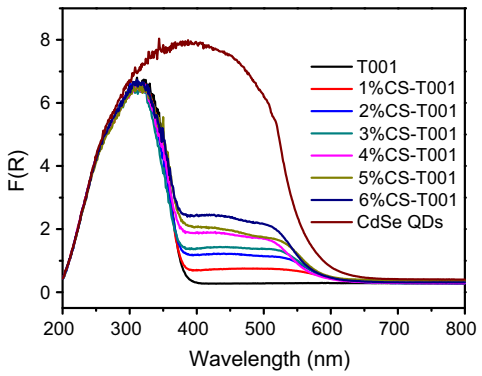

Fig. 4. UV–vis DRS spectra of T001, CdSe QDs and CS-T001 with different contents of CdSe QDs.

lattices are oriented perpendicular to each other with an equal lattice spacing of 0.189 nm, belonging to the (0 2 0) and (2 0 0) atomic planes. The fast Fourier transform (FFT) pattern of the same region (inset in Fig. 1b) can be indexed into diffraction spots of the [0 0 1] zone, indicating that the flat and square surface is (001) plane. The HRTEM image of the side face of T001 (Fig. 1c) directly shows that the lattice spacing parallel to the top and bottom facets is 0.235 nm, corresponding to the (0 0 1) plane of anatase TiO_2, which further demonstrates that the nanosheets are mainly exposed with {0 0 1} facets [5,44]. The detailed structural characterization of as-prepared CdSe QDs is displayed in Fig. S2. The results indicate that water soluble CdSe QDs has been successfully prepared, laying the foundation for the synthesis of CdSe QDs-decorated TiO_2. The TEM and HRTEM images of 5%CS-T001 are shown in Fig. 1d and e, respectively. By comparing Fig. 1a and d, we can see that the decoration of CdSe QDs does not have an obvious influence on the morphologies of TiO_2 nanosheets. For 5%CS-T001, small crystallites with sizes of several nanometers are clearly seen on the surface of TiO_2 nanosheets. As observed by HRTEM image in Fig. 1e, the lattice spacing of the small crystallite is detected to be 0.351 nm, corresponding to the (1 1 1) plane of cubic CdSe (JCPDS 19-0191). Meanwhile, the lattice spacing of 0.189 nm belongs to the (2 0 0) plane of anatase TiO_2 (JCPDS 21-1272). The energy dispersive X-ray spectroscopy (EDX, shown in Fig. 1f) demonstrates that the 5%CS-T001 is composed of Ti, O, F, Cd, Se and S elements. The elements of Ti, O, and F come from T001, while the elements of Cd, Se and S originate from the MAA-capped CdSe QDs which are decorated onto T001.

Fig. 2a shows the typical XRD patterns of T001 and T101. For T001 and T101, the diffraction peaks at $2\theta = 25.3^\circ, 37.8^\circ, 48.0^\circ, 53.9^\circ, 55.1^\circ$ and 62.7° can be indexed to (1 0 1), (0 0 4), (2 0 0), (1 0 5), (2 1 1) and (2 0 4) crystal planes of anatase TiO_2 (JCPDS 21-1272) respectively, indicating their pure anatase TiO_2 phase. Fig. 2b shows the typical XRD patterns of T001 and CS-T001 with different contents CdSe QDs. All peaks are indexed to T001, indicating that the decoration of CdSe QDs does not change the lattice structure of TiO_2. Moreover, no diffraction peaks assigned to CdSe QDs are found, which could be ascribed to the low content of CdSe QDs (max 6%) and their highly dispersion in T001. Raman spectroscopic measurement was conducted to further elucidate the components and structures of samples. As shown in Fig. 2c, both T001 and T101 are of the similar peaks appearing at 144, 197, 394, 514, and 636 cm^{-1}, indicating that both T001 and T101 belong to the typical anatase TiO_2 phase. Furthermore, the intensities of the E_g peaks at 144, 197 and 636 cm^{-1} of T001 are much weaker than those of T101, while the intensities of the B_{1g} peak at 394 cm^{-1} and the $A_{1g} + B_{1g}$ peak at 514 cm^{-1} of T001 are much stronger than those of T101. The results are consistent with previous reports [26,45,46], confirming the successful preparation of T001 and T101. Fig. 2d displays the Raman spectra of CdSe QDs and 5%CS-T001. The peak located at 205 cm^{-1} corresponds to the main peak of CdSe QDs [47]. For 5%CS-T001, besides the characteristic peaks belonging to T001, the peak located at 205 cm^{-1} can be clearly observed, which demonstrates the successful decoration of CdSe QDs.

To illustrate the chemical composition and valence states of various species, the XPS analysis of 5%CS-T001 was carried out. As shown in Fig. 3a, the peaks located at 459.0 and 464.7 eV correspond

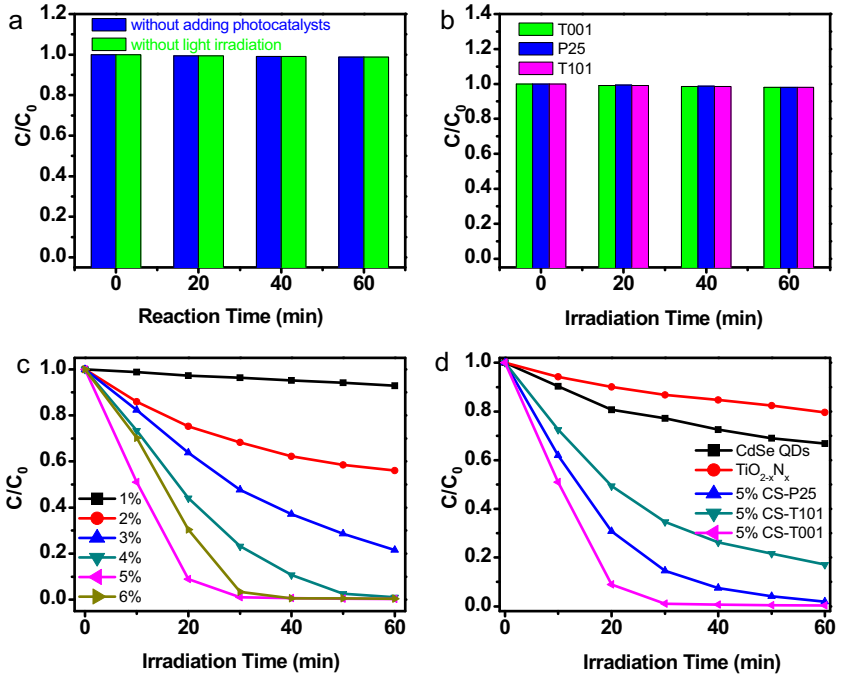

Fig. 5. Blank experiments for reduction of 4-NA without adding photocatalysts or light irradiation (a); photocatalytic activity for reduction of 4-NA over TiO_2 samples (T001, P25 and T101) (b), over CS-T001 with different contents of CdSe QDs (c) and over CdSe QDs, $TiO_{2-x}N_x$, 5%CS-P25, 5%CS-T101 and 5%CS-T001 (d) under visible light irradiation.

to Ti $2p_{3/2}$ and Ti $2p_{1/2}$, respectively, which are in good agreement with those in TiO_2 [15]. For O 1s spectrum (Fig. 3b), the three peaks at 530.4, 531.6 and 532.4 eV can be classified as the lattic oxygen, hydroxyl oxygen and adsorption oxygen, respectively [48]. In addition, the peaks of Cd $3d_{5/2}$ at 405.6 eV and Cd $3d_{3/2}$ at 412.3 eV (Fig. 3c) as well as Se $3d_{5/2}$ at 53.7 eV and Se $3d_{3/2}$ at 54.5 eV (Fig. 3d) confirm the existence of CdSe QDs [49] in 5%CS-T001.

The optical properties of the samples were studied from the UV–vis diffuse reflectance spectra (DRS) measurement. As can be readily seen in Fig. 4, pure T001 displays no spectral response in visible region due to its wide band gap, while pure CdSe QDs has absorption in visible range with a band edge at about 600 nm. All of the CdSe QDs-decorated T001 display the characteristic absorption of CdSe QDs and the absorption intensity goes up as the content of CdSe QDs increases. As is known, the visible light absorption is the precondition of materials possessing visible light photocatalytic activity. So the decoration of CdSe QDs should contribute greatly to the photocatalytic activity enhancement of CS-T001 under visible light irradiation.

3.2. Highly efficient visible light photocatalytic activity of CS-T001

3.2.1. Superior photocatalytic activity of CS-T001

The photocatalytic activities of samples have been evaluated by reduction of nitro aromatics 4-NA to corresponding amino aromatics with the addition of Na_2SO_3 as holes scavengers and N_2 purge under ambient conditions. Blank experiments under the same conditions show that no activity is observed in the absence of photocatalysts or light irradiation (Fig. 5a), indicating that the reaction is driven by a photocatalytic process. As shown in Fig. 5b, all TiO_2 samples (T001, P25 and T101) show negligible activity for reduction of 4-NA under visible light irradiation for 60 min, owing to their no absorption in visible region. In this study, we have synthesized CdSe QDs-decorated TiO_2, and mainly investigate their photocatalytic activities under visible light irradiation. Fig. 5c shows the photocatalytic performance of CS-T001 with different contents of CdSe QDs for reduction of 4-NA. With the content of CdSe QDs increases from 1% to 5%, the photocatalytic activity of CS-T001 increases obviously. However, when the content exceeds 5%, the activity starts to decrease. The 5%CS-T001 displays the optimal activity. Suitable content of CdSe QDs leads to both excellent visible light absorption and well particle dispersion on TiO_2, which are beneficial for high activity. However, too higher content of CdSe QDs would form overlapping agglomerates on the T001 surface (Fig. S3) and lower the activity for reduction of 4-NA. For 5%CS-T001, the photocatalytic conversion ratio of 4-NA reaches up to 98.9% under visible light irradiation for 30 min. The conversion of 4-NA to 4-PPD over 5%CS-T001 is monitored by UV–vis light adsorption spectroscopy and high performance liquid chromatography (HPLC), as shown in Fig. S2 and Fig. S3, respectively. According to Fig. S2, before visible light irradiation, there is only one absorption peak at about 380 nm, which corresponds to 4-NA. After irradiation for 30 min, the peak at about 380 nm disappears and two new peaks at about 305 nm and 240 nm appear, indicating that 4-NA is completely converted into *p*-phenylenediamine (PPD) [36]. Analogous results are also observed in the HPLC spectra (Fig. S3). It is clear to see that the impurity and intermediate peaks are very weak, suggesting that the very high selectivity is achieved for photocatalytic reduction of 4-NA to PPD.

To further evaluate the 5%CS-T001 photocatalyst, the photocatalytic activities for reduction of 4-NA over different samples are displayed in Fig. 5d. As can be seen clearly, the photocatalytic activities of samples follow the order 5%CS-T001 > 5%CS-P25 > 5%CS-T101 > CdSe QDs > $TiO_{2-x}N_x$. Obviously, 5%CS-T001 exhibits the best activity. $TiO_{2-x}N_x$, which has been reported to be an excellent visible light photocatalyst [43], shows poor activity for reduction of 4-NA. Although CdSe QDs has an obvious absorption in visible region, the high recombination rate of photo-generated electron–holes leads to low activity. For CdSe QDs-decorated TiO_2 samples, the photoresponse is extended into visible region. Moreover, high separation efficiency of photo-generated charge carriers can be achieved due to the electron transfer from CdSe QDs into TiO_2. As a result, CdSe QDs-decorated TiO_2 samples exhibit greatly enhanced activities than CdSe QDs. It should be particularly noted

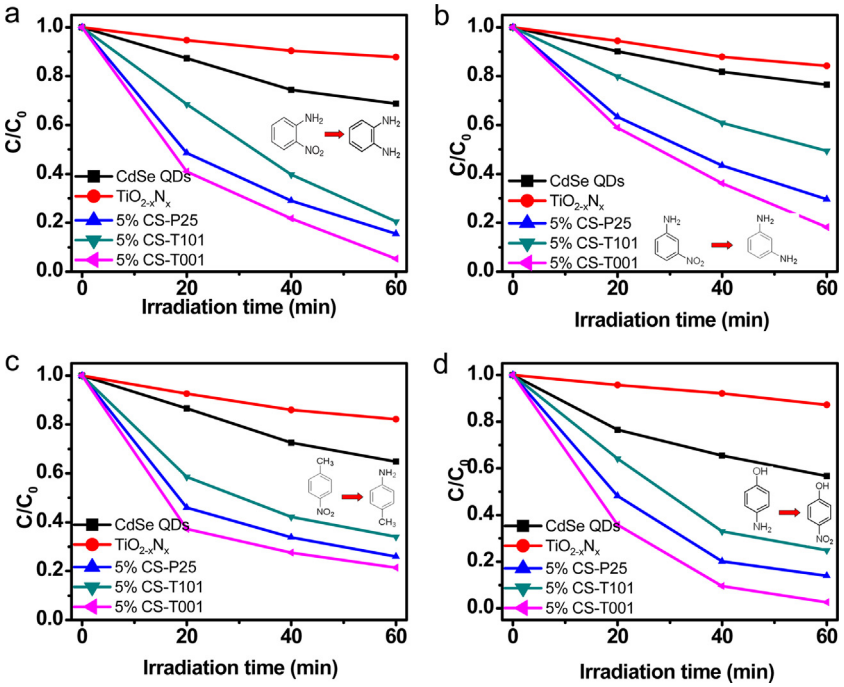

Fig. 6. Photocatalytic activity of CdSe QDs, $TiO_{2-x}N_x$, 5%CS-P25, 5%CS-T101 and 5%CS-T001 for reduction of different nitro aromatics under visible light irradiation: (a) 2-nitroaniline; (b) 3-nitroaniline; (c) 4-nitrotoluene and (d) 4-nitrophenol.

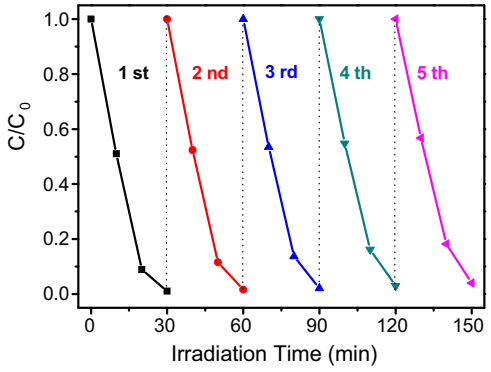

Fig. 7. The cycling photocatalytic activity of 5%CS-T001 for reduction of 4-NA under visible light irradiation.

that 5%CS-T001 performs much higher activity than 5%CS-T101, the reasons of which will be discussed in part 3.3 of this paper in detail.

Subsequently, to investigate if such an enhancement of photocatalytic activity is general for the reduction of nitro aromatics, we have also measured the photocatalytic activity of CdSe QDs, $TiO_{2-x}N_x$, 5%CS-P25, 5%CS-T101 and 5%CS-T001 for reduction of other nitro aromatics with different substituent groups, including 2-nitroaniline, 3-nitroaniline, 4-nitrotoluene and 4-nitrophenol. As displayed in Fig. 6a–d, the photocatalytic efficiencies follow the order 5%CS-T001 > 5%CS-P25 > 5%CS-T101 > CdSe QDs > $TiO_{2-x}N_x$, the same as that for reduction of 4-NA. These results indicate that the photocatalytic activity enhancement due to the decoration of CdSe QDs onto T001 is widely applicable toward reduction of nitro aromatics.

3.2.2. *Excellent photocatalytic stability of CS-T001*

Together with the photocatalytic activity, the stability of a photocatalyst is also of much importance for its application. The XRD and XPS patterns before and after photocatalytic reduction of 4-NA (shown in Fig. S4) indicate that the crystal structure and chemical state of 5%CS-T001 do not change after the photocatalytic reaction. Excitingly, Fig. 7 displays no significant loss of photocatalytic activity during five successive recycling tests for reduction of 4-NA over 5%CS-T001 under visible light irradiation. According to our previous report, CdSe QDs-modified TiO_2 suffered from photocorrosion upon photocatalytic degradation of MG due to the oxidation of CdSe by its own photogenerated holes [42]. In this study, the photogenerated holes are quenched by the addition of Na_2SO_3, which can efficiently prevent the photocorrosion of 5%CS-T001 during the photocatalytic reaction. These results demonstrate that our sample 5%CS-T001 can perform as a highly efficient and stable visible light-driven photocatalyst toward reduction of nitro aromatics with Na_2SO_3 as holes scavengers in N_2 atmosphere.

3.3. *Mechanism on the photocatalytic activity of CS-T001 for reduction of nitro aromatics*

In order to investigate the photocatalytic reaction mechanism, the effects of atmosphere and hole scavenger Na_2SO_3 on the photocatalytic reduction of nitro aromatics have been studied. For simplicity, reduction of 4-NA over 5%CS-T001 is still taken as an example and is shown in Fig. 8a. 4-NA is rapidly reduced to PPD in the presence Na_2SO_3 upon purging with N_2 under visible light irradiation. However, no significant reaction of 4-NA is observed after 30 min of visible light irradiation in the presence of Na_2SO_3 upon purging with either air (conversion 16.2%) or O_2 (conversion 1.5%). Evidently, N_2 atmosphere is indispensable for the photocatalytic reduction of 4-NA in this experiment. Under N_2 atmosphere, the formation of superoxide radicals ($O_2^{\bullet-}$) through trapping photogenerated electrons by O_2 is suppressed greatly. As a result, more electrons are available to participate in the reduction of 4-NA. In addition, the negligible reaction of 4-NA in the absence of Na_2SO_3 upon purging with N_2 (conversion 9.4%) indicates that the addition of Na_2SO_3 also plays a crucial role in the photocatalytic reduction of 4-NA. For the photocatalytic reduction of 4-NA, Na_2SO_3 as a hole scavenger can capture the photogenerated holes of photocatalyst (5%CS-T001), thereby reducing the recombination probability of photogenerated carriers and offering adequate opportunity for contact between photogenerated electrons and reactants (nitro aromatics). To prove that the reduction of nitro aromatics is driven by photogenerated electrons, we have further performed controlled experiments with the addition of $AgNO_3$ as an electron scavenger. As displayed in Fig. 8b, when 20 mg of $AgNO_3$ is added into the 4-NA reduction system, the photocatalytic activity of 5%CS-T001 is strongly inhibited, and negligible conversion of 4-NA is observed after the photocatalytic reaction. The results clearly confirm that the electrons are the main active species for the photocatalytic reduction of nitro aromatics.

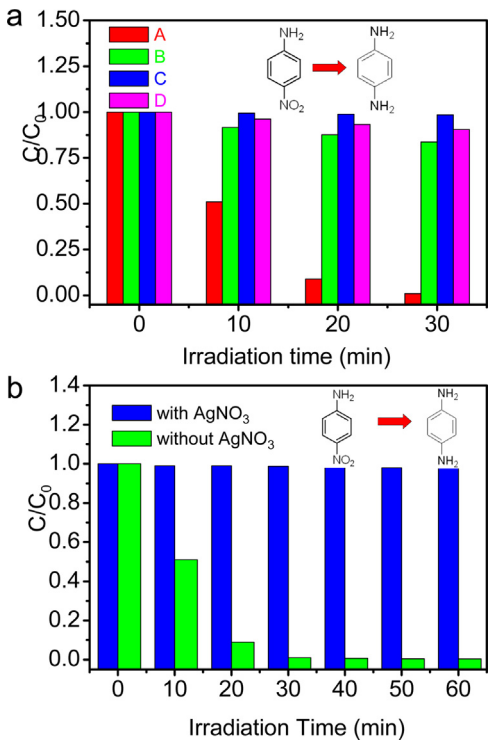

Fig. 8. (a) Photocatalytic activity of 5%CS-T001 for reduction of 4-NA under different conditions: (A) $Na_2SO_3 + N_2$, (B) Na_2SO_3 + air, (C) $Na_2SO_3 + O_2$, (D) N_2; (b) controlled experiments of 5%CS-T001 for reduction of 4-NA using $AgNO_3$ as electron scavenger under visible light irradiation with the addition of Na_2SO_3 as quencher for photogenerated holes in N_2 atmosphere.

In the system of CS-T001, T001 cannot be excited while CdSe QDs can be excited by visible light. So, T001 can serve as the accepted sites for photoelectrons generated from CdSe QDs and offer reaction sites for photocatalytic reduction of nitro aromatics. As is widely reported, the order of the average surface energies of anatase TiO_2 is {0 0 1} (0.90 J/m^2) > {1 0 0} (0.53 J/m^2) > {1 0 1} (0.44 J/m^2) [2–5]. Therefore, it can be deduced that the substrate T001 will offer highly active reaction sites due to the much higher surface energy of {0 0 1} facet than that of {1 0 1} facet.

DMPO spin-trapping ESR technique was introduced to investigate the photocatalytic reduction of nitro aromatics over the CdSe QDs-decorated TiO_2 photocatalysts. As displayed in Fig. 9a, the sextet of characteristic peaks of the DMPO-$O_2^{\bullet-}$ adducts can be detected in both 5%CS-T001 and 5%CS-T101 methanol suspensions

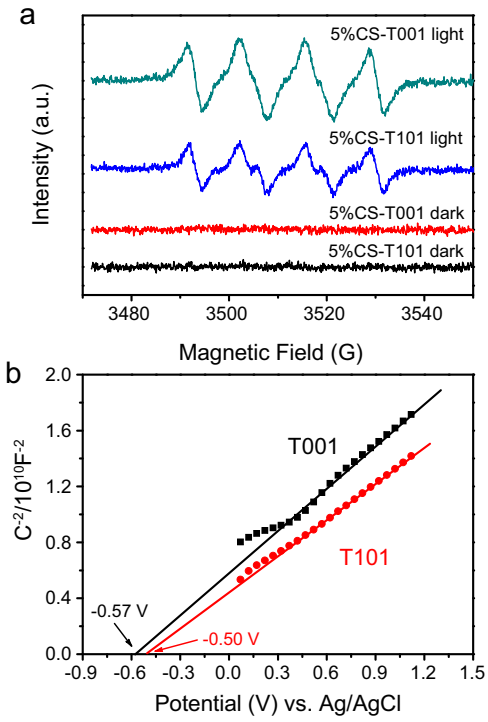

Fig. 9. (a) DMPO spin-trapping ESR spectra of 5%CS-T101 and 5%CS-T001 in methanol dispersion for DMPO-$O_2^{\bullet-}$ in dark or under visible light irradiation; (b) Mott–Schottky plots of T101 and T001.

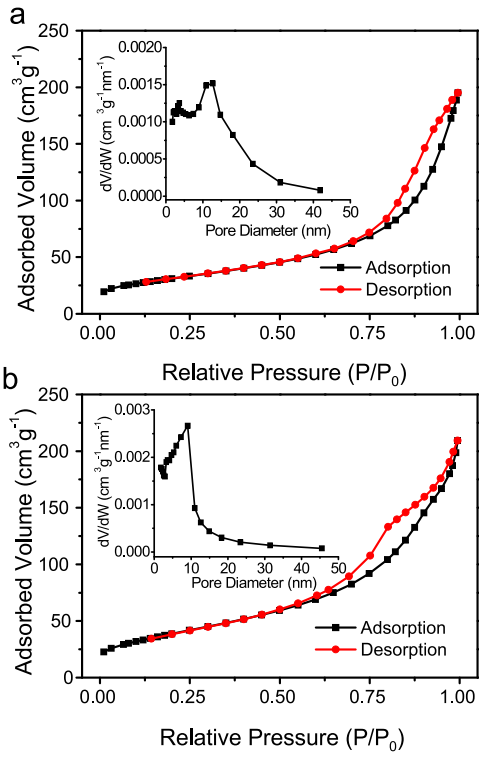

Fig. 10. Nitrogen adsorption–desorption isotherms and the corresponding pore size distribution curves (inset) of 5%CS-T001 (a) and 5%CS-T101 (b).

under visible light irradiation. As $O_2^{\bullet-}$ is formed by the reaction between photogenerated electrons and the absorbed O_2, the above results reflect that our photocatalysts can produce photogenerated electrons to reduce nitro aromatics to amino aromatics under N_2 atmosphere. Notably, the stronger intensity of DMPO-$O_2^{\bullet-}$ adducts indicates that the reducibility of electrons generated in 5%CS-T001 is stronger than that in 5%CS-T101, resulting in the much higher activity of 5%CS-T001. In addition to DMPO, another spin label TEMPO was also used for characterizing the electrons generated in photoexcited samples. According to the literature [50], the generation of photoinduced electrons and their reactivity can be easily monitored by observing changes in the ESR spectrum of TEMPO. The experiment results are shown in Fig. S7. Controlled experiment indicates that the ESR spectrum of TEMPO aqueous solution shows a stable signal having three peaks with intensity of 1:1:1 and the signal intensity was unchanged after mixing with catalysts before irradiation or irradiation without catalysts. The signal intensity decreased within 5 min of irradiation in the presence of 5%CS-T101; however, a more obvious reduction of ESR signal was observed upon irradiation of 5%CS-T001 for 5 min. These results indicate that the electrons are produced from photoexcited samples. Moreover, the reducibility of the photoelectrons generated from 5%CS-T001 is much stronger than that from 5%CS-T101. For the photocatalytic reduction of nitro aromatics under visible light irradiation, the electrons are generated from CdSe QDs and transferred to the conduction band of TiO_2. So, investigation of the conduction band potentials (V_{CB}) of different TiO_2 substrates can help us to realize the reducibility of electrons generated in CdSe QDs-decorated TiO_2 system. According to the Mott-Schottky plots shown in Fig. 9b, the flat band potentials (V_{fb}) of T001 and T101 are about −0.57 V and −0.50 V vs. Ag/AgCl, corresponding to −0.37 V and −0.3 V vs. normal hydrogen electrode (NHE), respectively. The positive slopes of the linear plots imply that T001 and T101 are *n*-type semiconductors, whose V_{CB} are very close (more negative by ~ −0.1 V) to their V_{fb}. Therefore, the V_{CB} of T001 and T101 are about −0.47 V and −0.4 V vs. NHE, respectively. It has been reported that the different arrangement and coordination of the surface atoms for the different exposed facets results in the different V_{CB} of T001 and T101 [51]. The more negative V_{CB} of T001 than that of T101 would probably lead to the stronger reducibility of electrons generated in 5%CS-T001 than that generated in 5%CS-T101.

To understand the effect of the surface area and porosity on the photocatalytic performance, the surface area and porosity of samples have been investigated. As can be seen in Table S1, the BET surface areas of all CdSe QDs-decorated T001 samples show little difference, which are all about 110 $m^2 g^{-1}$, indicating that the decoration of CdSe QDs do not bring evident influence on the BET surface area of T001. Moreover, Table S1 shows that the BET surface area of 5%CS-T001 (111 $m^2 g^{-1}$) is smaller than that of 5%CS-T101 (143 $m^2 g^{-1}$), indicating that the BET surface area cannot be mainly responsible for the highly efficient activity of 5%CS-T001. As shown in Fig. 10a, the N_2 adsorption–desorption isotherm of 5%CS-T001 belongs to type IV isotherm with a typical H3 hysteresis loop [52], which is reported for materials comprised of aggregates (loose assemblages) of plate-like particles forming slit-like pores [53]. Fig. 10b indicates that 5%CS-T101 also display type IV isotherm but with a H2 hysteresis loop, which is associated with the presence of pores with narrow mouths (ink-bottle pores) due to agglomerates of nanoparticles [53,54]. It is reported that the slit-like porous structures are very useful in photocatalytic reaction because they would provide efficient transport pathways to reactant and product molecules [16,54]. Therefore, the presence of slit-like porous structures formed by the aggregation of T001 nanosheets could be an important factor accounting for the highly efficient photocatalytic activity of 5%CS-T001 for reduction of nitro aromatics.

As is known, a necessary step for photocatalytic reaction is the generation and separation of photogenerated charge carriers. The photocurrent response and electrochemical impedance spectra (EIS) Nyquist plot, as very useful techniques to investigate the separation efficiency of photogenerated charge carriers [55], have been

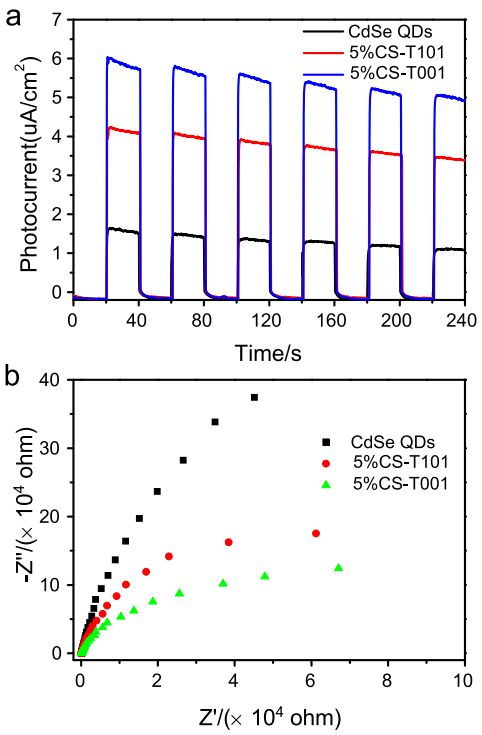

Fig. 11. Transient photocurrent responses under visible light irradiation (a) and electrochemical impedance spectroscopy (EIS) Nyquist plots (b) of CdSe QDs, 5%CS-T101 and 5%CS-T001.

performed. As shown in Fig. 11a, the significantly enhanced photocurrent responses for 5%CS-T001 suggest a more efficient transfer and separation of the photogenerated charge carriers for 5%CS-T001 than that for CdSe QDs and 5%CS-T101. It can be observed from Fig. 11b that 5%CS-T001 exhibits the smallest impedance arc radius among all samples, manifesting the best electrical conductivity, which will facilitate the improved transfer of photogenerated charge carriers and thus boost the photocatalytic efficiency. The photoluminescence (PL) spectra, resulting from the recombination of excited electrons and holes, can also reflect the separation efficiency of photogenerated electrons-holes [46,56]. As shown in Fig. S5, all samples exhibit a wide emission peak in visible region, which is attributed to the recombination of electrons and holes generated in CdSe QDs. As for CdSe QDs-decorated TiO_2 (5%CS-T001 and 5%CS-T101), the excited electrons would transfer from CdSe QDs to TiO_2, leading to the significantly reduced PL intensities. Notably, 5%CS-T001 shows a diminished PL intensity as compared to 5%CS-T101, suggesting the more efficient separation of photo-generated charge carries for 5%CS-T001 than that for 5%CS-T101. The results of photoelectrochemical tests and PL spectra are all well consistent with the trend of photocatalytic activity results. That is, the highly efficient photocatalytic activity of 5%CS-T001 for reduction of nitro aromatics could also be attributed to the fact that the decoration of CdSe QDs onto T001 would remarkably facilitate the interfacial charge transfer and improve the separation efficiency of photogenerated charge carriers.

On the basis of the above results, the reaction mechanism for photocatalytic reduction of nitro aromatics to amino aromatics over CS-T001 is proposed and displayed in Scheme 1. Under visible light irradiation, the electrons are excited from the valence band to the conduction band of CdSe QDs in CS-T001, leaving holes in the valence band. Due to the well matched energy band potentials and intimate interfacial contact between CdSe QDs and T001, the photogenerated electrons tend to transfer to the conduction band of T001, which inhibits the recombination of charge carriers and results in

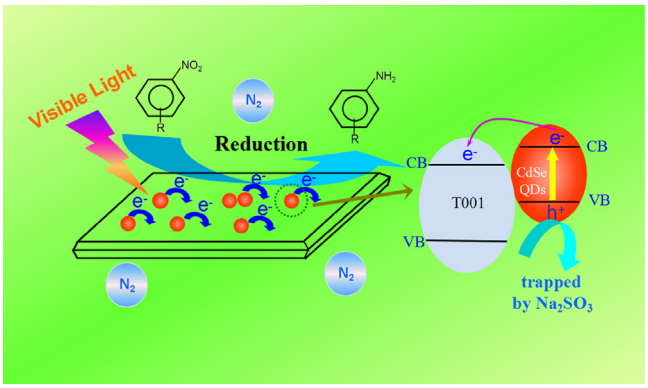

Scheme 1. Schematic diagram illustrating the photocatalytic reduction process of nitro aromatics to amino aromatics over CS-T001 under visible light irradiation.

efficient separation of electron–hole pairs. Simultaneously, the N_2 atmosphere and the addition of Na_2SO_3 as hole scavenger can guarantee that the nitro aromatics would not undergo the oxidation reaction. As a result, the nitro aromatics can be efficiently reduced to amino aromatics by accepting the photogenerated electrons from CS-T001 under visible light irradiation.

4. Conclusions

In summary, CS-T001 has been prepared through a facile hybridization method for the first time. According to the TEM, Raman spectra and XPS results, CdSe QDs has been successfully decorated on the surface of T001 nanosheets. CS-T001 exhibits highly efficient photocatalytic activity and excellent reusability toward reduction of nitro aromatics under visible light irradiation. It is demonstrated that the electrons generated from CdSe QDs and transferred to the conduction band of T001 are the main active species during the photocatalytic reduction process. Moreover, the substrate T001 also plays a vital role in the highly efficient activity of CS-T001. Firstly, T001 offers highly active reaction sites owing to the high surface energy of {0 0 1} facet; secondly, CS-T001 can generate electrons with stronger reducibility; thirdly, the aggregation of T001 nanosheets produces the porous structures with slit-like pores, providing efficient transport pathways to reactant and product molecules; fourthly, CS-T001 possesses much higher separation efficiency of photogenerated charge carriers. All these factors are beneficial for the enhancement of photocatalytic activity. We believe that this work could provide guided information and useful thought for the design and application of T001-based photocatalysts with excellent visible light photocatalytic activity.

Acknowledgment

This work was financially supported by the National Natural Science Foundation of China (21173047, 21373049).

Appendix A. Supplementary data

Supplementary data associated with this article can be found, in the online version, at http://dx.doi.org/10.1016/j.apcatb.2015.08.046.

References

[1] H.G. Yang, C.H. Sun, S.Z. Qiao, J. Zou, G. Liu, S.C. Smith, H.M. Cheng, G.Q. Lu, Nature 453 (2008) 638–641.
[2] C.Z. Wen, H.B. Jiang, S.Z. Qiao, H.G. Yang, G.Q. Lu, J. Mater. Chem. 21 (2011) 7052–7061.
[3] S. Liu, J. Yu, M. Jaroniec, Chem. Mater. 23 (2011) 4085–4093.

[4] S. Selçuk, A. Selloni, J. Phys. Chem. C 117 (2013) 6358–6362.
[5] X. Han, Q. Kuang, M. Jin, Z. Xie, L. Zheng, J. Am. Chem. Soc. 131 (2009) 3152–3153.
[6] G. Liu, C. Sun, H.G. Yang, S.C. Smith, L. Wang, G.Q. Lu, H.-M. Cheng, Chem. Commun. 46 (2010) 755–757.
[7] J. Yu, J. Low, W. Xiao, P. Zhou, M. Jaroniec, J. Am. Chem. Soc. 136 (2014) 8839–8842.
[8] Z. He, L. Jiang, D. Wang, J. Qiu, J. Chen, S. Song, Ind. Eng. Chem. Res. 54 (2015) 808–818.
[9] H. Wu, J. Ma, Y. Li, C. Zhang, H. He, Appl. Catal. B: Environ. 152–153 (2014) 82–87.
[10] C. Hu, X. Zhang, W. Li, Y. Yan, G. Xi, H. Yang, J. Li, H. Bai, J. Mater. Chem. A 2 (2014) 2040–2043.
[11] X. Zhou, F. Peng, H. Wang, H. Yu, Y. Fang, Chem. Commun. 48 (2012) 600–602.
[12] Y. Zhang, C. Li, C. Pan, J. Am. Ceram. Soc. 95 (2012) 2951–2956.
[13] J. Zhang, L. Qian, W. Fu, J. Xi, Z. Ji, J. Am. Ceram. Soc. 97 (2014) 2615–2622.
[14] D. Yang, Y. Li, Z. Tong, Y. Sun, Z. Jiang, Ind. Eng. Chem. Res. 53 (2014) 19249–19256.
[15] S. Zhu, S. Liang, Q. Gu, L. Xie, J. Wang, Z. Ding, P. Liu, Appl. Catal. B: Environ. 119–120 (2012) 146–155.
[16] J. Yu, L. Qi, M. Jaroniec, J. Phys. Chem. C 114 (2010) 13118–13125.
[17] L. Qi, J. Yu, M. Jaroniec, Phys. Chem. Chem. Phys. 13 (2011) 8915–8923.
[18] J. Yan, G. Wu, W. Dai, N. Guan, L. Li, ACS Sust. Chem. Eng. 2 (2014) 1940–1946.
[19] J. Long, H. Chang, Q. Gu, J. Xu, L. Fan, S. Wang, Y. Zhou, W. Wei, L. Huang, X. Wang, P. Liu, W. Huang, Energ. Environ. Sci. 7 (2014) 973–977.
[20] C. Hu, X. Zhang, X. Li, Y. Yan, G. Xi, H. Yang, H. Bai, Chem. -Eur. J. 20 (2014) 13557–13560.
[21] L. Zhang, D. Jing, X. She, H. Liu, D. Yang, Y. Lu, J. Li, Z. Zheng, L. Guo, J. Mater. Chem. A 2 (2014) 2071–2078.
[22] L. Gu, J. Wang, Z. Zou, X. Han, J. Hazard. Mater. 268 (2014) 216–223.
[23] V. Keller, F. Garin, Catal. Commun. 4 (2003) 377–383.
[24] W.-J. Ong, L.-L. Tan, S.-P. Chai, S.-T. Yong, A.R. Mohamed, ChemSusChem 7 (2014) 690–719.
[25] J. Hou, C. Yang, Z. Wang, S. Jiao, H. Zhu, Appl. Catal. B: Environ. 129 (2013) 333–341.
[26] L. Liu, X. Gu, C. Sun, H. Li, Y. Deng, F. Gao, L. Dong, Nanoscale 4 (2012) 6351–6359.
[27] H. Zhang, X. Quan, S. Chen, H. Yu, N. Ma, Chem. Mater. 21 (2009) 3090–3095.
[28] M.A. Hossain, J.R. Jennings, C. Shen, J.H. Pan, Z.Y. Koh, N. Mathews, Q. Wang, J. Mater. Chem. 22 (2012) 16235–16242.
[29] H. Zhang, K. Cheng, Y.M. Hou, Z. Fang, Z.X. Pan, W.J. Wu, J.L. Hua, X.H. Zhong, Chem. Commun. 48 (2012) 11235–11237.
[30] J. Hensel, G. Wang, Y. Li, J.Z. Zhang, Nano Lett. 10 (2010) 478–483.
[31] C. Wang, R.L. Thompson, J. Baltrus, C. Matranga, J. Phys. Chem. Lett. 1 (2009) 48–53.
[32] L. Yang, S. Luo, R. Liu, Q. Cai, Y. Xiao, S. Liu, F. Su, L. Wen, J. Phys. Chem. C 114 (2010) 4783–4789.
[33] M. Zhang, Y. Xu, J. Lv, L. Yang, X. Jiang, G. He, X. Song, Z. Sun, Nanoscale Res. Lett. 9 (2014) 1–7.
[34] S. Feng, S. Feng, J. Yang, J. Yang, M. Liu, M. Liu, Y. Liu, Y. Liu, J. Nanosci. Nanotechnol. 13 (2013) 787–792.
[35] S. Liu, Z. Chen, N. Zhang, Z.-R. Tang, Y.-J. Xu, J. Phys. Chem. C 117 (2013) 8251–8261.
[36] W. Wu, G. Liu, S. Liang, Y. Chen, L. Shen, H. Zheng, R. Yuan, Y. Hou, L. Wu, J. Catal. 290 (2012) 13–17.
[37] W. Wu, G. Liu, Q. Xie, S. Liang, H. Zheng, R. Yuan, W. Su, L. Wu, Green Chem. 14 (2012) 1705–1709.
[38] F.-X. Xiao, J. Miao, B. Liu, J. Am. Chem. Soc. 136 (2014) 1559–1569.
[39] K. Imamura, S. -i. Iwasaki, T. Maeda, K. Hashimoto, B. Ohtani, H. Kominami, Phys. Chem. Chem. Phys. 13 (2011) 5114–5119.
[40] W. Wu, L. Wen, L. Shen, R. Liang, R. Yuan, L. Wu, Appl. Catal. B: Environ. 130–131 (2013) 163–167.
[41] W. Wu, S. Liang, Y. Chen, L. Shen, H. Zheng, L. Wu, Catal. Commun. 17 (2012) 39–42.
[42] P. Wang, D. Li, J. Chen, X. Zhang, J. Xian, X. Yang, X. Zheng, X. Li, Y. Shao, Appl. Catal. B: Environ. 160–161 (2014) 217–226.
[43] R. Asahi, T. Morikawa, T. Ohwaki, K. Aoki, Y. Taga, Science 293 (2001) 269–271.
[44] J. Yu, J. Fan, K. Lv, Nanoscale 2 (2010) 2144–2149.
[45] F. Tian, Y. Zhang, J. Zhang, C. Pan, J. Phys. Chem. C 116 (2012) 7515–7519.
[46] Q. Xiang, J. Yu, M. Jaroniec, Nanoscale 3 (2011) 3670–3678.
[47] S. Wageh, Physica E 39 (2007) 8–14.
[48] F.-X. Xiao, ACS Appl. Mater. Interfaces 4 (2012) 7055–7063.
[49] J.E.B. Katari, V.L. Colvin, A.P. Alivisatos, J. Phys. Chem. 98 (1994) 4109–4117.
[50] W. He, H.-K. Kim, W.G. Wamer, D. Melka, J.H. Callahan, J.-J. Yin, J. Am. Chem. Soc. 136 (2014) 750–757.
[51] L. Ye, J. Liu, L. Tian, T. Peng, L. Zan, Appl. Catal. B: Environ. 134–135 (2013) 60–65.
[52] N. Zhang, Y.-J. Xu, Chem. Mater. 25 (2013) 1979–1988.
[53] M. Kruk, M. Jaroniec, Chem. Mater. 13 (2001) 3169–3183.
[54] Q. Xiang, K. Lv, J. Yu, Appl. Catal. B: Environ. 96 (2010) 557–564.
[55] Z. Chen, S. Liu, M.-Q. Yang, Y.-J. Xu, ACS Appl. Mater. Interfaces 5 (2013) 4309–4319.
[56] Y. Zhang, N. Zhang, Z.-R. Tang, Y.-J. Xu, ACS Nano 6 (2012) 9777–9789.